Construction and cosmic-ray test of the new inner drift chamber for BESIII

Yong-ji Xie(谢永骥)[1,2;1)] Zhong-hua Qin(秦中华)[1;2)] Xiao-yan Ma(马骁妍)[1] Jian Zhang(张建)[1]
Ling-hui Wu(伍灵慧)[1] Wan Xie(谢万)[1] Ming-yi Dong (董明义)[1] Jing Dong(董静)[1]
Xiao-lu Ji(季筱璐)[1] Xiao-shan Jiang(江晓山)[1] Qun Ou-yang(欧阳群)[1]
Ke-jun Zhu(朱科军)[1] Yuan-bo Chen(陈元柏)[1]

[1] Institute of High Energy Physics, Chinese Academy of Sciences, Beijing 100049, China
[2] University of Chinese Academy of Sciences, Beijing 100049, China

Abstract: A new inner drift chamber has been built which can replace the aged part of the BESIII drift chamber when needed. The design of the new inner drift chamber can minimize the ineffective area in the very forward and backward region and hence reduce the background event rate. With this design, the new inner drift chamber is expected to have a longer lifetime and improved performance due to the lower occupancy. The endplates and the cylinder were machined with high precision. Wire stringing was performed after the mechanical structure was assembled, and good quality of wire stringing was ensured by measurement of the tension and leakage current of the wires. After completion of the physical construction of the new chamber, a cosmic-ray test was carried out to test its performance. The results of the cosmic-ray test show that the new inner chamber achieves a spatial resolution of 127 μm and a dE/dx resolution of 6.4%, which satisfies the design specifications.

Keywords: BESIII, drift chamber, new inner drift chamber, cosmic-ray test

PACS: 29.40.Cs, 29.40.Gx **DOI:** 10.1088/1674-1137/40/9/096003

1 Introduction

As a large particle detector, the Beijing Spectrometer III [1] has been running since 2009. The drift chamber, as one of the major sub-detectors of BESIII, can provide good momentum resolution for charged particles by measuring their tracks in magnetic field. However, because of long-term exposure to high radiation from the accelerator, aging has been found in both sense wires and field wires of the drift chamber, especially in the inner part of the chamber [2]. Since BESIII will still operate for many years, a new inner drift chamber should be built, which will replace the old one whenever needed.

2 Requirements and design

The basic requirements for the new inner drift chamber is that the new chamber should achieve the same specifications as the old chamber, mainly for a spatial resolution of 130 μm and a dE/dx resolution of 6%∼7% [3]. Meanwhile, the new chamber is designed to have better performance when working in BESIII by reducing the background event rate. To achieve this, the ineffective area which is outside the required solid angle coverage(cosθ=0.93) should be minimized, so the new endplates have been elongated while the new cylinder is shortened, as shown in Fig. 1.

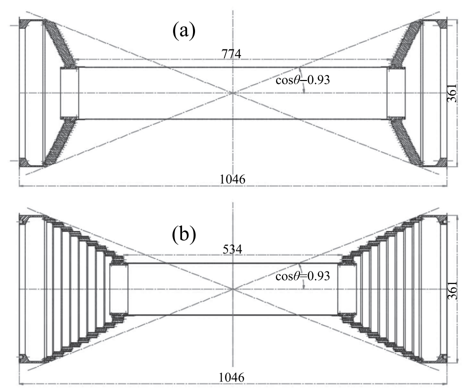

Fig. 1. Overview of the mechanical structure of the inner drift chamber: (a) the old inner chamber, (b) the new inner chamber.

The new endplate is composed of eight major steps, each containing one sense wire layer and one field wire

Received 22 February 2016, Revised 6 March 2016
1) E-mail: xieyj@mail.ihep.ac.cn
2) E-mail: qinzh@mail.ihep.ac.cn

Table 1. Lengths of wires for the inner drift chamber.

layer	wire length of the old chamber/cm	wire length of the new chamber/cm	background event rate reduction expected(%)
1	78.0	53.8	−31
2	79.2	58.0	−27
3	80.4	62.2	−23
4	81.6	66.4	−19
5	82.8	70.6	−15
6	84.0	74.8	−11
7	85.2	79.0	−7
8	86.4	83.2	−4

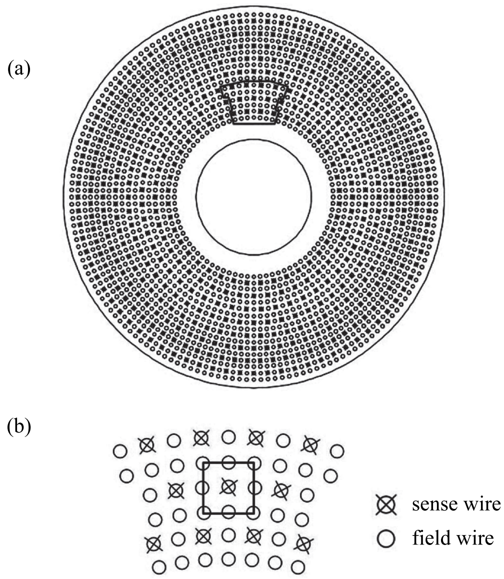

Fig. 2. (a) wire layer arrangement of the new chamber and (b) the drift cells of the chamber.

layer. The height of each step is 8 mm, which is 5 mm longer than the old one. The total thickness of the endplate is 189 mm, significantly thicker than the 73 mm of the old one. From the new design, the lengths of the wires have been shortened so the background event rate will be reduced, as shown in Table 1. The maximum reduction of background event rate is more than 30%, for the first sense wire layer.

Similar to the old chamber, the drift cells of the new chamber have a nearly square shape, as shown in Fig. 2, and the size of each cell is about 12 mm×12 mm with the sense wire located in the center, surrounded by eight field wires.

3 Machining and assembly

The material of the endplate is aluminum (type 7075) and the thickness is 25 mm after machining. There are a total of 2096 wire holes with a diameter of 3.2 mm in each endplate. All the 2096 holes were drilled on the single aluminum plate with special drilling tools. The position of each hole was surveyed and the results are shown in Fig. 3 for both endplates. All the holes have very high precision in positioning and the mean value of the tolerances is only 14 μm, which well meets the requirement of 25 μm.

The inner cylinder is made of carbon fiber with a thickness of 1.0 mm, and two layers of 100 μm-thick aluminum foils were pasted on both the inside and outside surfaces, as shown in Fig. 4. The gas tightness test showed that almost no pressure drops under 0.1 atm pressurization over 8 hours, and the stress test showed that the deflection is 0.09 mm for 300 kg axial load. The inner cylinder withstands the tension of all the wires, which is less than 100 kg.

The chamber is assembled with two endplates, one inner cylinder and two flanges, as shown in Fig. 5. The coordinates of the positioning holes on flanges and the wire holes on endplates were surveyed after assembly. The deviation is within 0.03 mm, which is much better than the design value of 0.05 mm, as shown in Fig. 6.

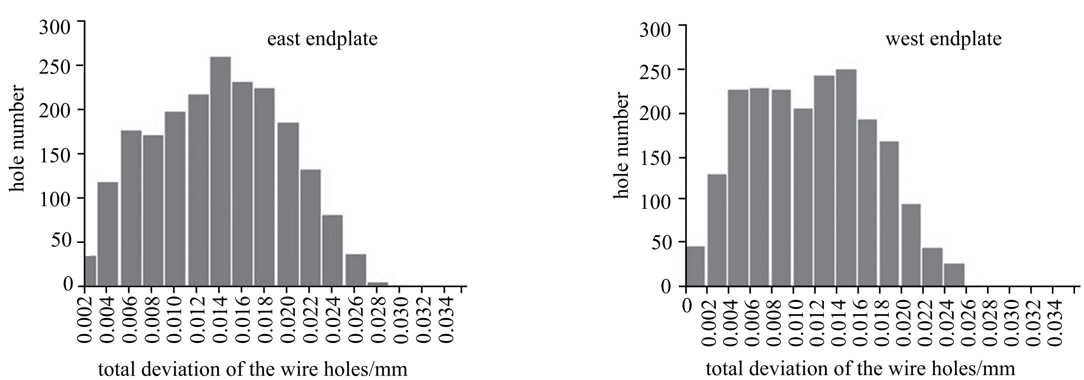

Fig. 3. Positioning tolerance of the wire hole.

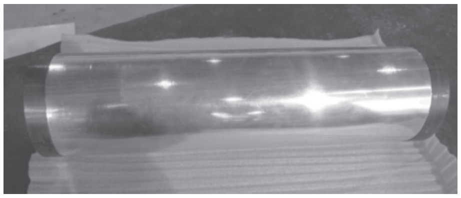

Fig. 4. The inner cylinder of the new inner drift chamber.

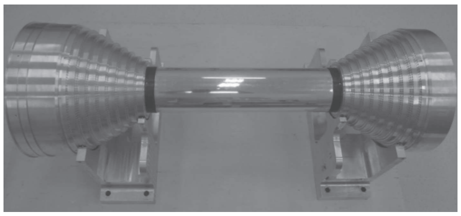

Fig. 5. The new inner drift chamber body after assembly.

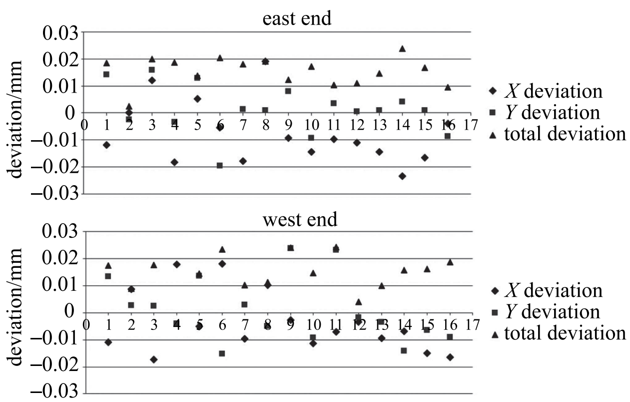

Fig. 6. Deviations of the positioning holes and wire holes.

4 Feed-through and wire

The feed-through is composed of a high voltage insulator made from injection molded plastic (LCP-A310) and a crimp pin, as shown in Fig. 7. The crimp pin is made of two concentrically nested tubes by a method of stretch forming, and the wire can pass through the inner tube and can be held after the tube is crimped. Aluminum pins are used for field wires and copper pins for the sense wires. The operating voltage of the feed-through is designed to be 2200 V and the leakage current should be less than 2 nA. All of the feed-throughs have been tested and the results show that the leakage current was lower than 0.5 nA for each feed-through during a period of 48 hours, where the humidity was about 55% and the high voltage was 2500 V, as shown in Fig. 8.

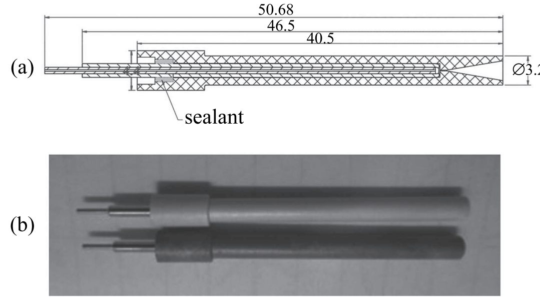

Fig. 7. The feed-through: (a) the mechanical drawing and (b) the prototype.

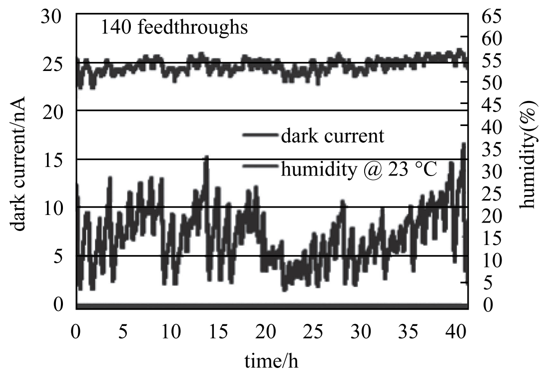

Fig. 8. Leakage current of feed-throughs, with 140 feed-throughs tested for each batch.

The field wires are 110 μm gold-plated aluminum and the sense wires are 25 μm gold-plated tungsten. The chamber is divided into 8 sense wire layers and 9 field wire layers. The numbers of sense wires and field wires in each layer are shown in Table 2. There are a total of 484 sense wires and 1612 field wires for the new inner drift chamber.

Table 2. Configuration of the wires of the new inner drift chamber.

layer	number of sense wires in sense wire layer(SS)	number of field wires in sense wire layer(SF)	number of field wires in field wire layer(FF)
1	40	40	80
2	44	44	88
3	48	48	96
4	56	56	112
5	64	64	128
6	72	72	144
7	80	80	160
8	80	80	160
8+	0	0	160

The wire parameters were measured. The linear density of the field wires is about 30.7×10^{-5} g/cm and that of the sense wires is about 9.3×10^{-5} g/cm. The maximum tension of the field wires before breaking is over

550g and that of the sense wire is over 120 g. Because the aluminum field wires will creep, 15% additional tension was applied for the stringing. Table 3 shows the configuration of wire tension, and the total tension is about 94 kg.

The wires were strung inside a class-10000 clean room to prevent possible contamination. To assure the uniformity of the wire tension, every wire was measured with an electrostatic method, and the results of measurements indicate that the non-uniformity of wire tension was less than 10%, as shown in Fig. 9. The leakage current was also measured and it was lower than 2 nA for each wire, as shown in Fig. 10.

In order to reduce the uncertainty of measurement, the wire tension and leakage current were measured three times, and the wires which did not meet the requirement were replaced with new ones. Figure 11 shows the new inner drift chamber with all the wires strung.

Table 3. Configuration of the wire tension.

layer	length/m	gravity sag/μm	tension/g	layer	length/m	gravity sag/μm	tension/g
1FF	0.534	30	43	5SS	0.708	45	13
1SS	0.540	30	11	5SF	0.708	45	50
1SF	0.540	30	44	6FF	0.744	45	55
2FF	0.576	30	50	6SS	0.750	45	15
2SS	0.582	30	13	6SF	0.750	45	56
2SF	0.582	30	51	7FF	0.786	50	55
3FF	0.618	35	49	7SS	0.792	50	15
3SS	0.624	35	13	7SF	0.792	50	56
3SF	0.624	35	50	8FF	0.828	50	62
4FF	0.660	35	56	8SS	0.834	50	16
4SS	0.666	35	15	8SF	0.834	50	62
4SF	0.666	35	57	8+FF	0.870	50	68
5FF	0.702	45	49				

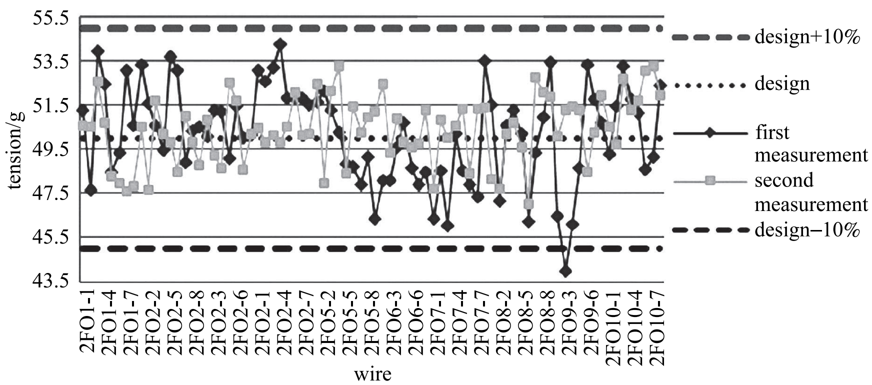

Fig. 9. Tension of the field wires in layer 2.

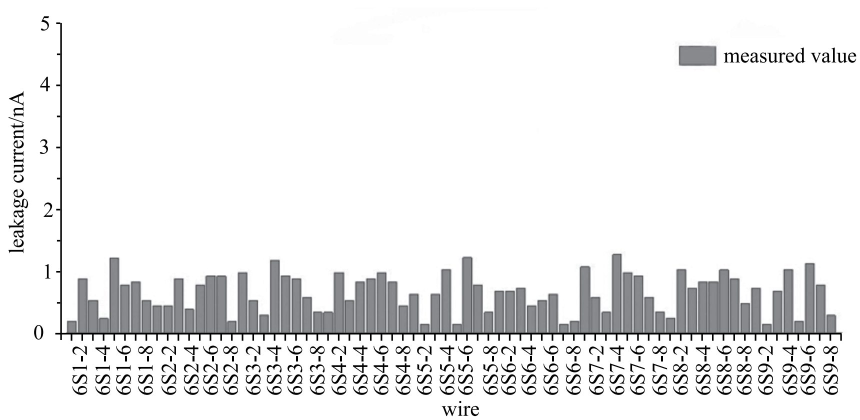

Fig. 10. Leakage current of the wires in layer 6.

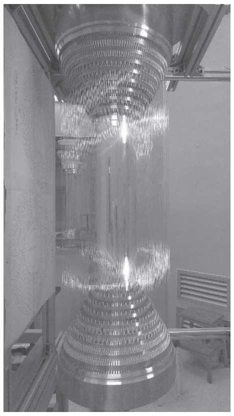

Fig. 11. The new inner drift chamber after wire stringing.

5 Cosmic-ray test

5.1 Setup of the cosmic-ray test

A cosmic-ray test without magnetic field is needed to test the performance of the chamber, and the chamber needs to be sealed for gas tightness, as shown in Fig. 12. For this purpose, a temporary outer cylinder made of aluminum was designed. This cylinder was connected to the chamber endplates by flanges, with O-rings in between for gas-tightness sealing. Moreover, to suppress noise being picked up by the front-end electronics, each end of the chamber had a 6 mm-thick aluminum box in which the front-end electronics were installed, as shown in Fig. 13.

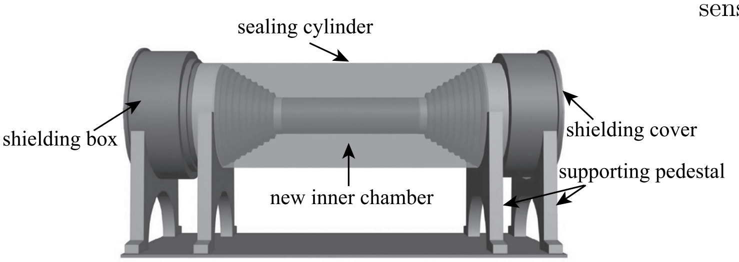

Fig. 12. The sealing and shielding of the new inner drift chamber for cosmic-ray testing.

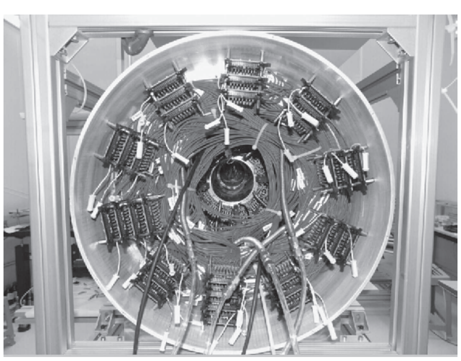

Fig. 13. The installation of front-end electronics.

In addition, a pair of scintillation counters were placed above and below the chamber. The counters were perpendicular to the direction of the wires and located in the center of the chamber to cover all the cells. The operating gas for the cosmic-ray test was a helium-based gas mixture of He and C_3H_8 (60:40), with a flow rate of about one chamber volume exchange per day. The high voltage system for the new chamber was provided by CAEN HV power supply of SY1527. A total of 13 channels of high voltage were powered for the sense wire layers. The electronics and DAQ system were the same as those used for the BESIII drift chamber [4]. The drift chamber under cosmic-ray testing is shown in Fig. 14.

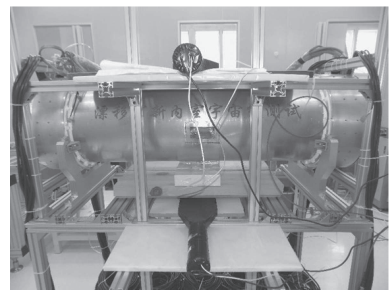

Fig. 14. The cosmic-ray test of new inner drift chamber.

5.2 Results from cosmic-ray test

5.2.1 Drift time distribution and X-T relation

Firstly, a typical cosmic-ray event after reconstruction by the chamber is shown in Fig. 15, with all the sense wire layers fired and fitted with a straight line.

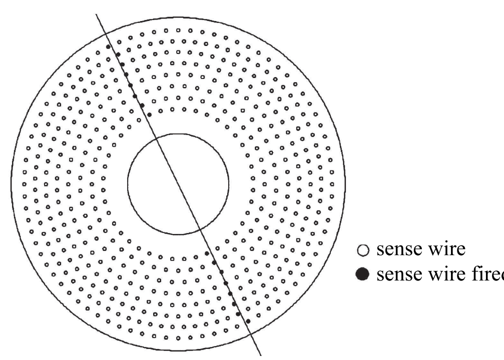

Fig. 15. A cosmic-ray event.

Figure 16 shows the drift time distribution. Due to the small drift cell size, the maximum drift time is about 300 ns. There is a second plateau which appears in the distribution, due to ionized electrons drifting from the area close to the cell edge, where the electric field is not uniform. Figure 17 shows the X-T scattering plot, which is smooth in most regions of the cell but nonlinear everywhere, with distortions at the boundary due to the distorted electric field there.

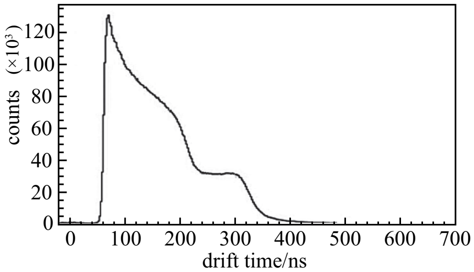

Fig. 16. Drift time distribution.

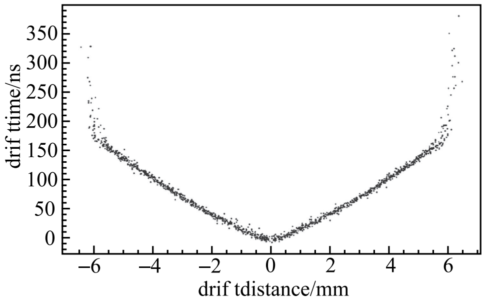

Fig. 17. Scatter plot of the X-T relation.

5.2.2 Spatial resolution

The spatial resolution of the new inner drift chamber is extracted from the residual distribution [5]. A dual Gaussian is used to fit this distribution and a spatial resolution of 127 μm is obtained for the high voltage of 2200 V, as shown in Fig. 18.

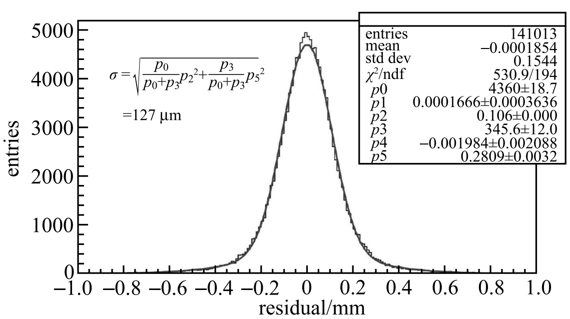

Fig. 18. Residual distribution.

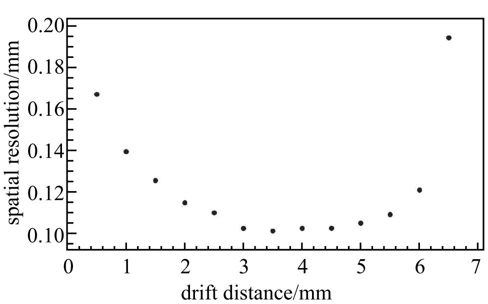

Fig. 19. Spatial resolution at different drift distances.

Figure 19 shows the spatial resolution as a function of distance from the sense wire. The best resolution is obtained in the middle area of the cell, with a sharp degradation at the cell boundary, which is also due to the distortions of the electric field in the boundary region.

5.2.3 dE/dx resolution

Figure 20 is a typical charge spectrum of cosmic-rays with the pedestal cut out, and the most probable value of the collected charge is about 400 fC.

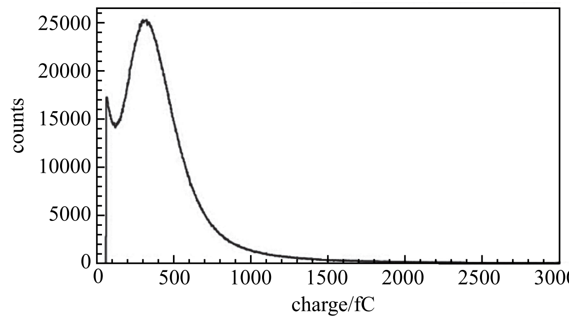

Fig. 20. Charge distribution.

Since the charge spectrum has a long Landau tail, the dE/dx resolution is extracted from a Gaussian fitting to the mean values of the charge measurements after truncation. Only a certain percentage (accepted fraction) of the total measurements is taken into account for the dE/dx resolution, to remove the effect of the Landau tail [6]. As shown in Fig. 21, the dE/dx resolution is 6.4% with 40 samples and an accepted fraction of 80%, for the high voltage of 2200 V.

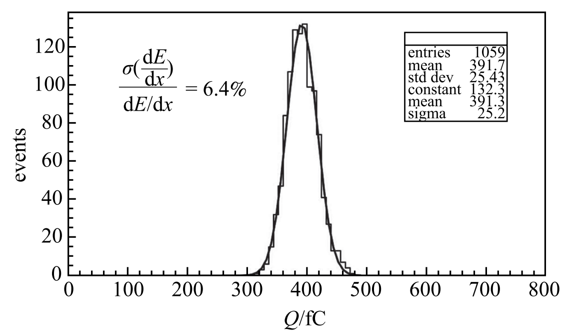

Fig. 21. The dE/dx resolution with a Gaussian fitting.

The dE/dx resolution dependence on the accepted fraction and the number of samples is shown in Fig. 22(a) and Fig. 22(b), respectively. For the gas mixture of He and C_3H_8 (60:40), the Landau tail is relatively small, so the best dE/dx resolution is obtained with an accepted fraction of 80%, while the more samples the better the resolution.

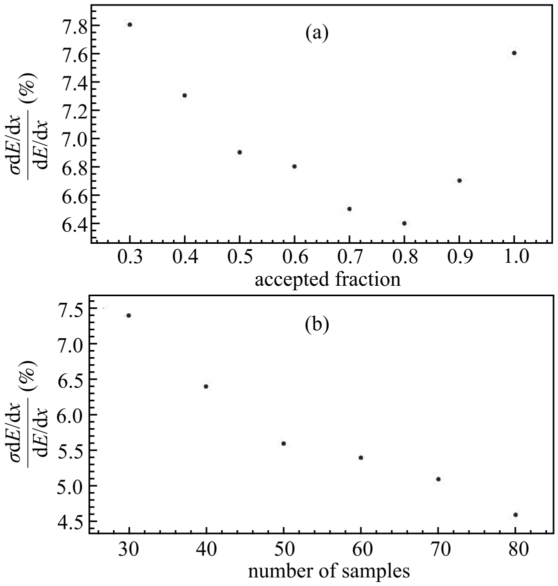

Fig. 22. (a) $\mathrm{d}E/\mathrm{d}x$ with different accepted fractions (b) $\mathrm{d}E/\mathrm{d}x$ with different numbers of samples.

6 Conclusions

The design of the new inner drift chamber can reduce the background event rate of the chamber and improve its lifetime and performance. The new inner chamber was constructed successfully including endplate and cylinder machining, feed-through fabrication, wire stringing and measurement. In order to test the performance of the new chamber, a cosmic-ray test was set up. A three month test was carried out and the results of the test indicate that the new chamber has excellent performance, including a spatial resolution of 127 μm and a $\mathrm{d}E/\mathrm{d}x$ resolution of 6.4%, which meets the design specifications. The new chamber can replace the old one when it is needed.

References

1 M. Ablikim, Z. H. An, J. Z. Bai et al, Nucl. Instrum. Methods A, **614**: 345–399 (2010)

2 M. Y. Dong, Q. L. Xiu, L. H. Wu et al, Chinese Physics C, **40(1)**: 16001–016001 (2016)

3 C. Chen, Y. B. Chen, M. Y. Dong et al, IEEE Nuclear Science Symposium Conference Record, **3**: 1844–1846 (2007)

4 Z. H. Qin, Y. B. Chen, H. Y. Sheng et al, Nucl. Instrum. Methods A, **571**: 612–621 (2007)

5 J. B. liu, C. Chen, Y. B. Chen et al, Chinese Physics C, **29(4)**: 387–392 (2005)

6 D.Jeanne, P. Lazeyras, I. Lehraus et al, Nucl. Instrum. Methods A, **111**: 287–300 (1973)